AWARD NUMBER: W81XWH-17-1-0352

TITLE: Targeting the acidic microenvironment of prostate cancer using chemical shift-based, clinically translatable hyperpolarized ^{13}C MRI biomarkers

PRINCIPAL INVESTIGATOR: Céline Taglang

CONTRACTING ORGANIZATION: University of California, San Francisco (UCSF)

REPORT DATE: Nov 2019

TYPE OF REPORT: Final

PREPARED FOR: U.S. Army Medical Research and Materiel Command
Fort Detrick, Maryland 21702-5012

REPORT DOCUMENTATION PAGE

Form Approved
OMB No. 0704-0188

1. REPORT DATE	2. REPORT TYPE	3. DATES COVERED
Nov 2019	Final	1 Aug 2017 – 31 Jul 2019

4. TITLE AND SUBTITLE
Targeting the Acidic Microenvironment of Prostate Cancer Using Chemical Shift-Based, Clinically Translatable Hyperpolarized 13C MRI Biomarkers

5a. CONTRACT NUMBER

5b. GRANT NUMBER
W81XWH-17-1-0352

5c. PROGRAM ELEMENT NUMBER

6. AUTHOR(S)
Céline Taglang

E-Mail: celine.taglang@ucsf.edu

5d. PROJECT NUMBER

5e. TASK NUMBER

5f. WORK UNIT NUMBER

7. PERFORMING ORGANIZATION NAME(S) AND ADDRESS(ES)

University of California San Francisco, San Francisco
1855 Folsom St STE 425
San Francisco CA 94103-4249

8. PERFORMING ORGANIZATION REPORT NUMBER

9. SPONSORING / MONITORING AGENCY NAME(S) AND ADDRESS(ES)

U.S. Army Medical Research and Materiel Command
Fort Detrick, Maryland 21702-5012

10. SPONSOR/MONITOR'S ACRONYM(S)

11. SPONSOR/MONITOR'S REPORT NUMBER(S)

12. DISTRIBUTION / AVAILABILITY STATEMENT

Approved for Public Release; Distribution Unlimited

13. SUPPLEMENTARY NOTES

14. ABSTRACT

During the first year of research period, efforts were focused on the synthesis of new classes of hyperpolarized (HP) ^{13}C agents for probing interstitial pH (pH_e). Synthesis of [^{13}C,^{15}N]ACES still needs to be optimized but we already reported that deuterium labeling of one the building blocks, [1-^{13}C,2-$^{2}H_2$]glycine, led to a significant increase of its relaxation time T_1 (+ 25% compared to the non-deuterated ^{13}C-labeled glycine). We are convinced that application of this strategy to ACES will also improve its T_1, which is a critical property in the development of efficient chemical shift-dependent imaging agents. Optimization of the synthesis of [2-^{13}C,$^{2}H_{10}$]DEMA was successful with high chemical yields and purity. [^{13}C,^{2}H] labeling is also a key aspect in the potential for DEMA as a candidate for high spatial resolution *in vivo* pH_e mapping. Indeed, DEMA has one of the longest relaxation times measured for HP molecules. We reported the development of DEMA: it exhibits a large pH-dependent ^{13}C chemical shift over the physiological range. We demonstrated that co-polarization with [1-^{13}C,$^{2}H_9$]tert-butanol accurately measured pH *via* ^{13}C NMR and magnetic resonance spectroscopic imaging in phantoms. *In vivo* experiments enabled us to evaluate DEMA as a clinically translatable HP ^{13}C MRI biomarker.

15. SUBJECT TERMS
Prostate cancer, hyperpolarization, magnetic resonance imaging, isotopic labeling, interstitial pH, acidic microenvironment

16. SECURITY CLASSIFICATION OF:			17. LIMITATION OF ABSTRACT	18. NUMBER OF PAGES	19a. NAME OF RESPONSIBLE PERSON
a. REPORT	b. ABSTRACT	c. THIS PAGE			19b. TELEPHONE NUMBER *(include area code)*
Unclassified	Unclassified	Unclassified	Unclassified	19	USAMRMC

TABLE OF CONTENTS

	Page
1. Introduction	4
2. Keywords	4
3. Accomplishments	5
4. Impact	10
5. Changes/Problems	11
6. Products	12
7. Participants & Other Collaborating Organizations	14
8. Special Reporting Requirements	14
9. Appendices	15

INTRODUCTION:

Prostate cancer has a heterogeneous disease course. Distinguishing between the different phenotypes of prostate cancer is an important problem for clinical oncologists. Non-invasive biomarkers that would not only characterize prostate cancer aggressiveness but also predict response to therapy would be of enormous benefit to patients. One potential prognostic imaging biomarker is acidic interstitial pH, which has been shown to be associated with local invasion and metastases in a variety of cancers. The central hypothesis of this proposal is that low interstitial pH is strongly correlated with both tumoral lactate generation and tumor aggressiveness. We propose to investigate, using hyperpolarized (HP) ^{13}C magnetic resonance spectroscopy (MRS), the relationship of lactate export to extracellular matrix acidification, establish pH as a critical determinant of cancer aggressiveness and use new HP platforms to target tumor acidity with the long-term aim to develop new clinically-translatable HP imaging approaches. The Specific aim 1 is to develop new classes of HP ^{13}C agents for probing interstitial pH. The Specific Aim 2 is to validate the efficiency of the new HP ^{13}C agents for MRI. The Specific aim 3 is to investigate the relationship between HP lactate generation and acidic interstitial pH. We will correlate HP pH maps to lactate generation and efflux and show grade-dependent changes in tumoral acidity.

1. KEYWORDS:

Prostate cancer
Hyperpolarization
Magnetic resonance imaging
Isotopic labeling
Interstitial pH
Acidic microenvironment
Carbon-13
Deuterium
N-(2-Acetamido)-2-aminoethanesulfonic acid (ACES)
Diethylmalonic acid (DEMA)

2. ACCOMPLISHMENTS:

What were the major goals of the project?

Specific Aim 1: Develop new classes of HP ^{13}C agents for probing interstitial pH

- Subtask 1: Optimize HP ACES as a chemical-shift dependent ^{13}C imaging agent
  Target date: February 1, 2018
  Completion date: -
  Percentage of completion: 70%
- Subtask 2: Develop dicarboxylate sensors as pH-sensitive HP imaging probes
  Target date: February 1, 2018
  Completion date: August 31, 2018
  Percentage of completion: 100%
- Milestone(s) Achieved: Synthesis and ^{13}C,^{2}H labeling of HP ^{13}C agents
  Target date: February 1, 2018
  Completion date: -
  Percentage of completion: 90%

Specific Aim 2: Validate these new HP ^{13}C agents in vivo using a gold standard (^{31}P-APP)

- Subtask 1: Validate chemical shift-based pH imaging methods using ^{31}P-APP
  Target date: August 1, 2018
  Completion date: -
  Percentage of completion: 0%
- Subtask 2: Demonstrate HP probe response to simple modulations of tumoral pH
  Target date: August 1, 2019
  Completion date: -
  Percentage of completion: 50%
- Milestone(s) Achieved: Imaging and in vivo studies on [^{13}C,^{2}H] ACES and [1-^{13}C, $^{2}H_{10}$] DEMA
  Target date: August 1, 2019
  Completion date: -
  Percentage of completion: 25%

Specific Aim 3: Investigate the relationship between HP lactate generation and acidic interstitial pH

- Subtask 1: Correlate HP pH maps to lactate generation and efflux
  Target date: August 1, 2019
  Completion date: -
  Percentage of completion: 0%
- Subtask 2: Show grade-dependent changes in tumoral acidity
  Target date: August 1, 2019
  Completion date: -
  Percentage of completion: 0%
- Milestone(s) Achieved: Rigorously investigate the precise mechanism implying lactate export and low interstitial pH
  Target date: August 1, 2019
  Completion date: -

What was accomplished under these goals?

Specific Aim 1: Develop new classes of HP ^{13}C agents for probing interstitial pH

- Subtask 1: Optimize HP ACES as a chemical-shift dependent ^{13}C imaging agent.

Our group previously demonstrated that hyperpolarized [^{13}C,^{15}N] ACES could be used to determine pH using ^{13}C magnetic resonance spectroscopy [1]. Indeed this probe was applied to pH measurement in an NMR spectrometer and in a chemical shift imaging experiment on a clinical 3 T MRI scanner. However, with a relaxation time T_1 (or hyperpolarized lifetime in solution, which is a major limitation in hyperpolarized ^{13}C magnetic resonance spectroscopy) of 18 seconds at 11.7 T and 25 seconds at 3 T, ACES represents an interesting candidate for pH imaging *via* HP ^{13}C MRS but needs to be improved. One approach to increase T_1 is the substitution of ^{1}H with ^{2}H (or D) atom. In April 2018, we reported a robust and selective late-stage deuteration methodology and applied it to ^{13}C-enriched amino and alpha hydroxy acids to increase spin–lattice relaxation constant T_1 for hyperpolarized ^{13}C magnetic resonance imaging. This methodology was based on the regioselective deuteration, at the α-position of aliphatic alcohols and sugars, developed by Sajiki *et al*., and the use of ruthenium on carbon [2]. For the five substrates with ^{13}C-labeling on the C1-position ([1-^{13}C]alanine, [1-^{13}C]serine, [1-^{13}C]lactate, [1-^{13}C]glycine, and [1-^{13}C]valine), significant increase of their T_1 was observed at 3 T with deuterium labeling (+26%, +22%, +16%, +25% and +29%, respectively). Remarkably, in the case of [2-^{13}C]alanine, [2-^{13}C]serine and [2-^{13}C]lactate, deuterium labeling led to a greater than four fold increase in T_1. [1-^{13}C,2-^{2}H]alanine, produced using this method, was applied to in vitro enzyme assays with alanine aminotransferase, demonstrating a kinetic isotope effect [3, attached article in Appendix 1].

As shown in the scheme 1 of Appendix 2, [1-^{13}C,2-$^{2}H_2$]glycine was a building block in the synthetic strategy of [^{15}N,^{13}C,$^{2}H_4$]ACES **2**. As we showed an increase of +25% of its T_1 compared to [1-^{13}C]glycine **3**, which is a building block of the non deuterium-labelled [^{15}N,^{13}C]ACES **1**, we are confident that deuterium labelling of [^{15}N,^{13}C]ACES will improve its T_1. The three first synthetic steps of [^{15}N,^{13}C]ACES **1** (BOC-protection, amide formation and BOC-deprotection) led to the key intermediate **6** with satisfying chemical yields (scheme 1b of Appendix 2). Unfortunately, the last step (nucleophilic substitution) resulted in the formation of the desired [^{15}N,^{13}C]ACES **1** with a low chemical yield. We think that the pH of the reaction, which must remain constant, is a key parameter for this reaction to succeed. Moreover, The purification step by crystallization represents also a challenge: a major quantity of the target compound stay solubilized which leads to the low chemical yield. New attempts to improve the yield of this reaction were under investigation in our laboratory until the target date (February 1, 2018) but they were not successful. This step represents the only challenge of our approach in the synthesis of [^{15}N,^{13}C,$^{2}H_4$]ACES **2**. Indeed, we already checked the feasibility of deuterium labeling on [^{15}N,^{13}C]ACES **1**: the target molecule was obtained with high chemical yield (89%) and isotopic enrichment (99% on the α-position of ^{13}C).

- Subtask 2: Develop dicarboxylate sensors as pH-sensitive HP imaging probes

In 2017, we reported the development of hyperpolarized [2-^{13}C,D_{10}]diethylmalonic acid, which exhibits a large pH-dependent ^{13}C chemical shift over the physiological range. We demonstrated that co-polarization with [1-^{13}C,D_9]*tert*-butanol accurately measured pH via ^{13}C NMR and magnetic resonance spectroscopic imaging in phantoms [4, attached article in Appendix 3]. The synthesis of DEMA was based on two steps with a total chemical yield of 75%: alkylation of [2-^{13}C]diethylmalonate with [D_5]bromoethane and saponification using NaOH. In conclusion, our synthetic strategy did provide the target probe DEMA. Synthetic access to this desired proposed substrate is a significant milestone for the progress of the project.

Specific Aim 2: Validate these new HP ^{13}C agents in vivo using a gold standard (^{31}P-APP)
As the synthesis of [^{15}N,^{13}C,$^{2}H_4$]ACES **2** appeared more challenging than expected (specific aim 1, subtask 1), we focused our efforts for the development of chemical shift-based pH imaging with DEMA.

- Subtask 1: Validate chemical shift-based pH imaging methods using ^{31}P-APP

We anticipate that a chemical shift-based HP method will allow high spatial-resolution pH mapping in our murine models, similar to what has been previously reported for ^{1}H and ^{31}P-based spectroscopic techniques. We planned to compare our HP probes to pH calculations using ^{31}P-APP, using both phantom and in vivo pH mapping in the TRAMP model. Nonetheless, while ^{31}P-APP is considered as a gold standard, it still has numerous limitations preventing its clinical translation, such as non-uniform distribution throughout the tumours. Thus, we decided to use microelectrodes as a validating method, even if it can be considered as an invasive method which could alter the measured pH values. Indeed, we think that microelectrodes represented a more efficient and straightforward method.

Methods
Hyperpolarization: DEMA was prepared and co-polarized with [1-^{13}C,D_9]tert-butanol as previously described by Korenchan *et al*. [4].
In vivo pH measurement in mouse kidneys at 3 T: a tail vein injection of HP DEMA and *t*BuOH (50 µL each co-polarized then diluted to 45 mM) into 5 healthy mice was performed, followed by imaging of a slice containing the kidneys, 25 and 35 seconds after completion of the injection. ^{13}C-bicarbonate (co-polarize with urea) was subsequently injected to compare pH values.
Results
A tail vein injection of HP DEMA and tBuOH into a healthy mouse showed a strong signal from the kidneys with a noticeable amount in the blood pool (Figure 1b, Appendix 4). We discovered two peaks of DEMA within the same kidney voxel forming two pH clusters (pH 7.43 and 6.41, $n = 1$) consistent with data from literature [6]. Indeed, zymonic acid co-polarized with urea showed peaks in the same type of imaging conditions with pH of 7.40 ± 0.01 and 6.55 ± 0.03 ($n = 4$ rats, mean ± s.d.). The measured pH values showed good agreement with the average voxel pH measured using HP [^{13}C]bicarbonate (pH 6.77, Figure b).
Conclusion
The fact that DEMA, instead of using a ratiometric method, uses differences in chemical shifts to determine the pH, allows for the detection of multiple pH compartments within the same voxel, contrary to ^{13}C-bicarbonate that shows a mean pH. Similar to the prior study employing zymonic acid, we propose that these two peaks with pH of 7.43 and 6.41 arise from the cortical and calyx/ureter compartments, respectively. Interestingly, DEMA has a higher *in vitro* T_1 at 3 T than zymonic acid: 84 and 43-51 seconds, respectively. As polarization lifetime is a major limitation of using ^{13}C-labelled probes for *in vivo* applications, DEMA represents a pH imaging candidate for clinical translation.

- Subtask 2: Demonstrate HP probe response to simple modulations of tumoral pH

Two TRAMP mice were used for this part of the study to evaluate the feasibility of imaging the modulation of pH on this model with DEMA copolarized with [1-^{13}C,D_9]tert-butanol at 3 T. While the signal from [1-^{13}C,D_9]tert-butanol was clearly observable, the signal from DEMA was only visible in one or two voxels which displayed a pH value of 7.07 which is not high enough to clearly localize the the tumor. We suppose that this pH value is more an average of the pH coming from the tumor and the rest of the tissues. We hypothesized that measuring the pH at higher field (14 Tesla) would enable us to better observe the DEMA signal (see "Methods" in the "Subtask 1" section for details).

A tail vein injection of HP DEMA and tBuOH into a healthy mouse at 14 T showed a strong signal from the right kidney (Appendix 5). We observed two peaks of DEMA within the same kidney voxel forming two pH clusters (pH 7.29 and 6.18, *n = 1*) consistent with data from literature. We then decided to continue our study at 14 T with another mouse model (RCC: renal cell carcinoma).

In vivo pH measurement in RCC mice kidneys at 14 T: a tail vein injection of HP DEMA and *t*BuOH (50 µL each co-polarized then diluted to 45 mM) into 6 RCC mice was performed, followed by imaging of a slice containing the kidneys, 25 and 40 seconds after completion of the injection. Microelectrodes were subsequently used to compare pH values. Appendix 6 shows an example of signals obtained at timepoint 40 s: we observed two peaks of DEMA within the same kidney voxel forming two pH clusters (pH 7.22 and 6.28, *n = 1*). Similar clusters were observed for the five other mice.

We tried to inject galbumin in two more RCC mice after injection of DEMA to suppress to vascular signal and, consequently, improve the measurement of acidic pH, but more assays are necessary to develop an adapted protocol involving DEMA and galbumin.

To evaluate the response of DEMA depending on pH modulation, we administrated sodium bicarbonate via oral gavage (1M, 1 cc maximum) 2 hours prior to induction of anesthesia and imaging to 3 healthy mice. Unfortunately, at 3 T, we couldn't observe any pH value higher than 7.41, which is similar to the results obtained on non bicarbonate-treated healthy mice (see subtask 1).

More assays would be necessary to confirm DEMA response to pH modulation. We showed that DEMA injections enabled us to measure pH in different compartments of mice kidneys consistent with data from litterature, so we think that DEMA represent a great potential HP ^{13}C agent for microenvironment of prostate tumors.

Specific Aim 3: Investigate the relationship between HP lactate generation and acidic interstitial pH

- Subtask 1: Correlate HP pH maps to lactate generation and efflux

Nothing to report

- Subtask 2: Show grade-dependent changes in tumoral acidity

Nothing to report

What opportunities for training and professional development has the project provided?

The purpose of this grant application was to build upon my training as a chemist by taking on a project in prostate cancer biomarker development that more heavily emphasizes magnetic resonance imaging. I joined the Wilson lab at UCSF to strengthen my training in biomarker and drug development by taking on a project that focused on studying new hyperpolarized ^{13}C agents, their biocompatibility and their potential for near-term translation. I also deliberately chose to work on prostate cancer, owing to the established role of nuclear imaging and medicine in standard of care.

To broaden my knowledge base, there are several mechanisms available for my education inside and outside the lab. I have a serious peer group of chemists and chemical biologists that have been very helpful in teaching me radiochemistry, preclinical pharmacology and animal work. Moreover, Dr. Dave Korenchan, who obtained his Ph.D. with Pr. John kurhanewicz and has more than three years of expertise in the development of hyperpolarized ^{13}C MRS imaging agent, taught me how to optimize the formulations ACES and DEMA, the hyperpolarization process and the treatment of the data.

During the first year of the project, I mainly focused on research and further educating myself on the background and goals of my project (synthesis, formulation of samples for injection), but I also could summarize the data, described in the specific aim 1, for manuscript submissions [3 and 4], and submit an accepted poster to ISMRM annual meeting (Paris, June 2018). As the second year of the project was focused on hyperpolarized 13-carbon MRI/S and handling of animals, I was trained by my colleagues and specialists on every step of my studies (hardware such as spectrometer parametrization, software such as Topspin, anesthesia and euthanasia of animals, data processing).

During the two years of funding period I was co-mentored by Drs. Wilson (primary mentor), Flavell (co-mentor) and Kurhanewicz (secondary mentor). We met together every week to discuss my research progress and plans to convert the data into high impact publications and long term grant support from public mechanisms.

How were the results disseminated to communities of interest?

Nothing to report.

What do you plan to do during the next reporting period to accomplish the goals?

Nothing to report.

4. **IMPACT:**

What was the impact on the development of the principal discipline(s) of the project?

Nothing to report.

What was the impact on other disciplines?

Nothing to report.

What was the impact on technology transfer?

Nothing to report

What was the impact on society beyond science and technology?

Nothing to report.

5. CHANGES/PROBLEMS:

Nothing to report.

Actual or anticipated problems or delays and actions or plans to resolve them

Nothing to report.

Changes that had a significant impact on expenditures

Nothing to report.

Significant changes in use or care of human subjects, vertebrate animals, biohazards, and/or select agents

Nothing to report.

Significant changes in use or care of human subjects

Nothing to report

Significant changes in use or care of vertebrate animals

Nothing to report

Significant changes in use of biohazards and/or select agents

Nothing to report.

6. PRODUCTS: *List any products resulting from the project during the reporting period. If there is nothing to report under a particular item, state "Nothing to Report."*

- **Publications, conference papers, and presentations**

Journal publications.

Céline Taglang, David E. Korenchan, Cornelius von Morze, Justin Yu, Chloé Najac, Sinan Wang, Joseph E. Blecha, Sukumar Subramaniam, Robert Bok, Henry F. VanBrocklin, Daniel B. Vigneron, Sabrina M. Ronen, Renuka Sriram, John Kurhanewicz, David M. Wilson and Robert R. Flavell. *Late-stage deuteration of ^{13}C-enriched substrates for T_1 prolongation in hyperpolarized ^{13}C MRI*. Chemical Communications, **54**, 5233 (2018). Published. DOI: 10.1039/c8cc02246a. Acknowledgement of federal support: yes.

Books or other non-periodical, one-time publications.

Nothing to report.

Other publications, conference papers and presentations.

Poster presentation:
Céline Taglang, David E. Korenchan, Cornelius von Morze, Chloé Najac, Joseph E. Blecha, Justin Yu, Sukumar Subramaniam, Robert Bok, Henry F. VanBrocklin, Renuka Sriram, John Kurhanewicz, David M. Wilson, Robert R. Flavell. *A late-stage deuteration method for T_1 prolongation and enhanced in vivo signal to noise ratio of hyperpolarized ^{13}C substrates*. Annual Meeting ISMRM-ESMRMB 2018, Paris Expo Porte de Versailles, Paris, France.

- **Website(s) or other Internet site(s)**

Nothing to report.

- **Technologies or techniques**

Nothing to report.

- **Inventions, patent applications, and/or licenses**

Nothing to report.

- **Other Products**

Nothing to report.

7. PARTICIPANTS & OTHER COLLABORATING ORGANIZATIONS

What individuals have worked on the project?

No change.

Has there been a change in the active other support of the PD/PI(s) or senior/key personnel since the last reporting period?

Nothing to report.

What other organizations were involved as partners?

Nothing to report.

8. SPECIAL REPORTING REQUIREMENTS

Nothing to report.

9. APPENDICES:

Appendix 1

ChemComm

COMMUNICATION

View Article Online
View Journal | View Issue

Cite this: *Chem. Commun.*, 2018, 54, 5233

Received 21st March 2018,
Accepted 30th April 2018

DOI: 10.1039/c8cc02246a

rsc.li/chemcomm

Late-stage deuteration of ^{13}C-enriched substrates for T_1 prolongation in hyperpolarized ^{13}C MRI†

Céline Taglang, David E. Korenchan, Cornelius von Morze, Justin Yu, Chloé Najac, Sinan Wang, Joseph E. Blecha, Sukumar Subramaniam, Robert Bok, Henry F. VanBrocklin, Daniel B. Vigneron, Sabrina M. Ronen, Renuka Sriram, John Kurhanewicz, David M. Wilson and Robert R. Flavell *

A robust and selective late-stage deuteration methodology was applied to ^{13}C-enriched amino and alpha hydroxy acids to increase spin–lattice relaxation constant T_1 for hyperpolarized ^{13}C magnetic resonance imaging. For the five substrates with ^{13}C-labeling on the C1-position ([1-^{13}C]alanine, [1-^{13}C]serine, [1-^{13}C]lactate, [1-^{13}C]glycine, and [1-^{13}C]valine), significant increase of their T_1 was observed at 3 T with deuterium labeling (+26%, 22%, +16%, +25% and +29%, respectively). Remarkably, in the case of [2-^{13}C]alanine, [2-^{13}C]serine and [2-^{13}C]lactate, deuterium labeling led to a greater than four fold increase in T_1. [1-^{13}C,2-^{2}H]alanine, produced using this method, was applied to *in vitro* enzyme assays with alanine aminotransferase, demonstrating a kinetic isotope effect.

Magnetic resonance imaging employing hyperpolarized substrates (HP MRI) has recently emerged as a powerful tool for studying metabolism in cells, animal models and patients.[1–9] Polarization of substrates can be realized through a variety of mechanisms including dissolution dynamic nuclear polarization (DNP),[10] parahydrogen induced polarization (PHIP),[11,12] or signal amplification by reversible exchange (SABRE).[13] While these are versatile methods that allow for real time imaging of metabolism, the short lifetime of the hyperpolarized signal, which decays exponentially based upon the spin lattice relaxation time T_1, remains one of the key limiting factors in the implementation of this technology. The most widely used HP ^{13}C probe is [1-^{13}C]pyruvate, a key metabolic intermediate, which has a T_1 of 67 s at 3 T. However, other ^{13}C nuclei, especially those with directly attached protons, are not feasible HP ^{13}C probes due to very short T_1's (less than 5 s).[14] One approach to increase T_1 is the substitution of ^{1}H with ^{2}H (or D), a quadrupolar nucleus with a gyromagnetic ratio γ about 6.5-fold smaller than the one for ^{1}H.[15–29] This use of deuterated substrates has proved particularly fruitful in the case of SABRE[13] and PHIP[11,12] methods. This approach is effective when dipolar ^{13}C–^{1}H coupling contributes substantially to T_1 relaxation. Fortunately, in the case of pyruvate, the incorporation of deuterium is straightforward owing to lack of stereocenters.[30] However, the synthesis of multiply labelled molecules containing stereocenters including both ^{13}C and ^{2}H is generally both expensive and time consuming, and most isotopically enriched molecules require multi-step syntheses. Therefore, a robust method for incorporation of deuterium in the final step of synthesis would be generally valuable in the field of HP MRI.

For the synthesis of deuterated molecules, late-stage isotopic exchange has several advantages over a synthetic pathway from enriched building blocks. Numerous methods based on homogeneous or heterogeneous catalysts for H/D exchange have already been described, but the development of a deuteration methodology with mild reaction conditions, high selectivity and deuterium incorporation is still a challenge.[31,32] In order to develop [^{13}C,^{2}H] labelled probes for HP MRI, we considered the regioselective deuteration, at the α-position of aliphatic alcohols and sugars, developed by Sajiki *et al.*, as a straightforward way to the deuterium labelling of ^{13}C-substrates with attached O or N.[33,34] In this manuscript, we report the application of this methodology to a variety of ^{13}C-enriched compounds, enabling high incorporation yields with retention of configuration, and demonstrate a significant increase in T_1 of the resulting deuterated substrates. One of the probes, [1-^{13}C,2-^{2}H]alanine, was studied in an *in vitro* enzymatic assay with alanine aminotransferase (ALT), revealing a deuterium kinetic isotope effect.

Initially, we evaluated the performance of the labelling methodology with a variety of labelled substrates including α-amino and hydroxy acids. We performed the one-step deuterium labelling reaction on position C2 of several commercial ^{13}C-labeled substrates (Scheme 1 and Table 1). Reactions were incubated in D_2O in the presence of RuC 5% (40 wt%), under H_2, overnight, at 80 °C (Table S1, ESI†). Efficient deuterium incorporation on position C2 (95–97%) was observed for aliphatic amino acids [1-^{13}C,2-^{2}H] and [2-^{13}C,2-^{2}H]alanine (**1** and **6**), [1-^{13}C,2-^{2}H$_2$]glycine **4** and [1-^{13}C,2-^{2}H]valine **5**, with enantiomeric

Department of Radiology and Biomedical Imaging, University of California, San Francisco, USA. E-mail: robert.flavell@ucsf.edu

† Electronic supplementary information (ESI) available: Reagents and procedures for deuteration reaction, deuterium incorporation quantification, characterization for compounds **1** to **8**, experimental details for T_1 measurements in solution, *in vivo* and *in vitro* enzyme experiments. See DOI: 10.1039/c8cc02246a

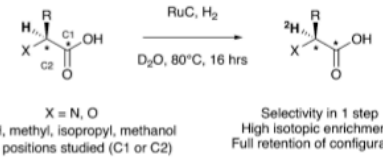

Scheme 1 Regioselective catalytic deuterium labelling *via* $^{1}H/^{2}H$ exchange using ruthenium on carbon (RuC).

Table 1 Structures of ^{13}C-enriched molecules after deuterium enrichment. The bracketed number indicates the isotopic enrichment determined by ^{1}H, ^{13}C NMR and HRMS (analyses described in the ESI). ee: enantiomeric excess

Molecule	Structure	Chemical yield (%)	ee (%)
^{13}C on position C1 and ^{2}H on position C2			
[1-^{13}C,2-^{2}H]alanine **1**	[97]	99	99
[1-^{13}C,2,3-^{2}H$_3$]serine **2**	[26] [52]	78	98
[1-^{13}C,2-^{2}H]lactate **3**	[97]	98	86
[1-^{13}C,2-^{2}H$_2$]glycine **4**	[97]	79	—
[1-^{13}C,2-^{2}H]valine **5**	[95]	53	99
^{13}C on position C2 and ^{2}H on position C2			
[2-^{13}C,2-^{2}H]alanine **6**	[97]	89	99
[2-^{13}C,2,3-^{2}H$_3$]serine **7**	[65] [90]	77	98
[2-^{13}C,2-^{2}H]lactate **8**	[98]	99	94

excesses greater than 99%. Isotopic enrichments on position C2 of [1-^{13}C,2-^{2}H] and [2-^{13}C,2-^{2}H]sodium lactate (**3** and **8**) were 97% and 98%, respectively, with lower enantiomeric excesses (86 and 94%). Moderate chemical yield on [1-^{13}C,2-^{2}H] valine **5**, 53%, may be due to its lower solubility in D_2O. Enantiomeric excess was 98% for both [1-^{13}C,2-^{2}H] and [2-^{13}C,2-^{2}H]serine (**2** and **7**) whereas chemical yields were 78% and 77%, respectively. Their lower isotopic enrichments on position C2 (52 and 90%) may be due to the additional deuterium labelling on their position C3.

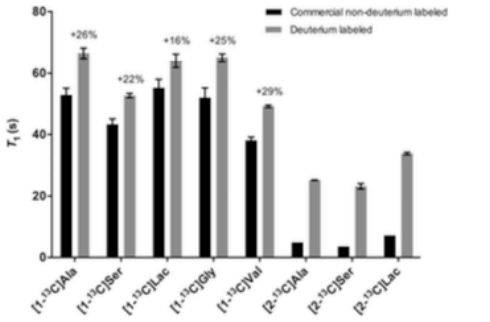

Fig. 1 T_1 relaxation times at 3 T for proton and deuterium-labelled ^{13}C-substrates (n = 3, ±s.d., $p < 0.02$). Due to very low polarization for commercial non-deuterium labeled [2-^{13}C]alanine, [2-^{13}C]serine and [2-^{13}C]lactate, T_1 could not be evaluated using hyperpolarized methods, and inversion-recovery was used at 11.7 T: T_1 = 4.9 s, 3.6 s and 7.2 s, respectively.

In a few cases, side reactions were encountered which led to decomposition of the desired product (ESI†). Taken together with prior reports,[27,35] our data indicate that this is a versatile method for deuterium incorporation in biologically relevant molecules.

In order to determine the impact of deuterium incorporation on T_1, we then prepared the labelled substrates for hyperpolarization. Solutions of 4 to 6 M substrate with 1 to 1.2 equivalents NaOH and 23 to 24 mM free radical (OX063) were prepared for hyperpolarization using DNP.[36] Following polarization, T_1 measurements were performed on a 3 T preclinical MR scanner. Deuterium substitution at the C2 position yielded significant improvements of the T_1 with ^{13}C at the C1 position, ranging from 16–29% (Fig. 1). The relatively modest improvement in T_1 yielded larger signal gains at later time points. For example, in the case of [1-^{13}C]alanine, deuteration yielded an increase in signal to noise ratio of 60% at 90s after the start of the experiment (Fig. S68c, ESI†). Remarkably, in the case of [2-^{13}C,2-^{2}H]alanine **6**, [2-^{13}C,2,3-^{2}H]serine **7** and [2-^{13}C,2-^{2}H]lactate **8**, deuterium labelling led to a greater than four-fold increase in T_1. Due to rapid signal decay on [2-^{13}C]alanine, [2-^{13}C]serine and [2-^{13}C]lactate, their T_1 could not be measured using a hyperpolarized method[36] and were instead assayed using an inversion recovery-sequence. Part of the reason why the T_1 gains due to deuteration are relatively limited is because of chemical shift anisotropy (CSA) which is likely the dominant relaxation mechanism at 3 T.[37,38] Therefore, at 1.5 T, there could be further improvements in T_1 prolongation.[39]

We then evaluated the T_1 of one of our substrates, [1-^{13}C,2-^{2}H]-alanine **1**, in an *in vivo* experiment in a mouse model and compared its properties with those of [1-^{13}C]alanine. MR measurements where performed on a preclinical 3 T scanner (Fig. S71, ESI†). 300 μL of 80 mM solutions of hyperpolarized [1-^{13}C]alanine and [1-^{13}C,2-^{2}H]alanine **1** were injected intravenously immediately followed by dynamic acquisition of ^{13}C MRS spectra. As expected, based on the *in vitro* studies, we found an increase in the apparent *in vivo* T_1 at 3 T, from 32 s, for [1-^{13}C]alanine, to 42 s, for [1-^{13}C,2-^{2}H]alanine **1**.

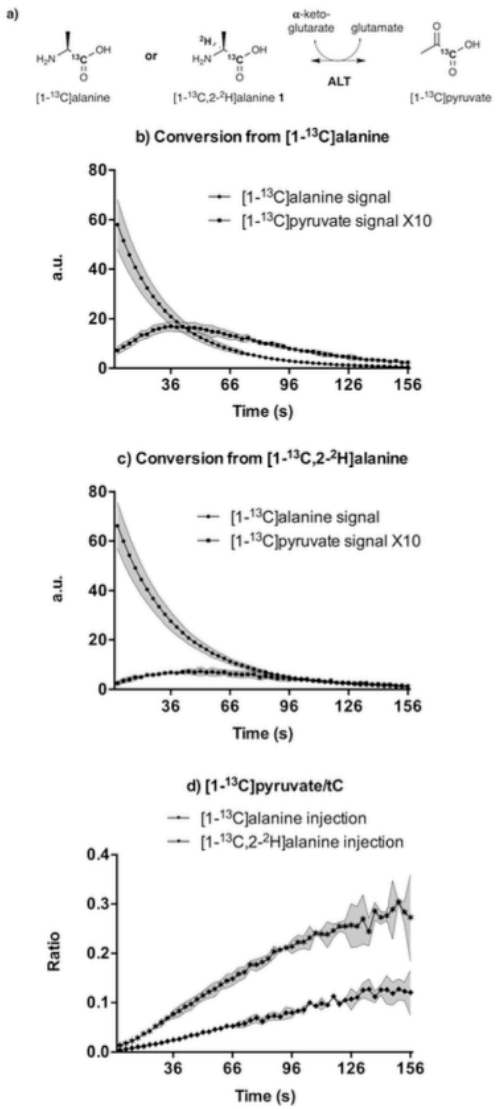

Fig. 2 Influence of deuterium labelling on [1-^{13}C]pyruvate formation after conversion from [1-^{13}C]alanine and from [1-^{13}C,2-^{2}H]alanine **1** in solution in the presence of ALT enzyme. (a) Metabolic pathways of hyperpolarized [1-^{13}C]alanine and [1-^{13}C,2-^{2}H]alanine **1** *via* ALT. (b and c) Time courses of integrated spectra showing the evolution of HP [1-^{13}C]alanine,[1-^{13}C,2-^{2}H]alanine **1** and their metabolite [1-^{13}C]pyruvate (normalized peak integrations) (n = 3, ±s.d.). For clarity, pyruvate integrals were ten-fold upscaled. Shaded areas denote the experimental error bars. Spectral acquisition started 11 s (b) and 10 s (c) after incubation of the HP probe and the enzyme solution in an NMR tube. (d) Measurements of [1-^{13}C]pyruvate/total ^{13}C-labeled signals (tC) ratios (n = 3, ±s.d.).

As a demonstration of the utility of the deuteration method, we next applied the labelled alanine probes in an *in vitro* enzyme assay using alanine transaminase (ALT). ALT is an abundant enzyme and a biomarker for liver disease, which converts alanine and α-ketoglutarate to pyruvate and glutamate, respectively (Fig. 2a). Previous reports have studied this enzyme both *in vitro* and *in vivo* using hyperpolarized ^{13}C methods.[36,40,41] Therefore, we developed an assay for the detection of ^{13}C pyruvate production by incubation of polarized [1-^{13}C]alanine or [1-^{13}C,2-^{2}H]alanine **1** with α-ketoglutarate, glutamate and ALT based on prior reports.[42] As expected, ^{13}C pyruvate was rapidly formed during the time course of the hyperpolarized experiment (Fig. 2b–d). Furthermore, the initial rate of pyruvate signal growth, which approximates the forward conversion rate, was about 2.42-fold lower for the [1-^{13}C,2-^{2}H]alanine **1** as compared with the [1-^{13}C]alanine (n = 3 each, $p < 0.002$, neutral pH). This agrees closely with the previously reported kinetic isotope effect of 2.3.[42] In order to confirm these findings, we fit the dynamic alanine and pyruvate MRS data to a kinetic model accounting for HP signal exchange between protonated and deuterated [1-^{13}C]alanine and [1-^{13}C]pyruvate pools as well as signal loss due to RF sampling and T_1 loss (Fig. S72, ESI†).[43] We thus obtained pseudo-first order rate constants of $(1.87 \pm 0.174) \times 10^{-3}$ s^{-1} (n = 3) and $(0.736 \pm 0.015) \times 10^{-3}$ s^{-1} (n = 3) for protonated and deuterated alanine, respectively. This difference in kinetic rates suggested a kinetic isotope effect of 2.53, in close agreement with our previous analysis and with the literature.[42]

In summary, these data indicate that the RuC labelling method represents a versatile method for high-yield deuteration of ^{13}C labelled substrates, ideal for application to hyperpolarized ^{13}C MRI. When the deuterium was incorporated adjacent to a ^{13}C-enriched carbonyl, the effect on T_1 prolongation was moderate, ranging from 16–29%. In contrast, when applied to ^{13}C nuclei with directly attached protons ([2-^{13}C,2-^{2}H]alanine **6**, [2-^{13}C,2,3-^{2}H]serine **7** and [2-^{13}C,2-^{2}H]lactate **8**), an approximately 4-fold increase in T_1 was observed. To further study the behavior of doubly-enriched substrates, we applied [1-^{13}C]alanine and [1-^{13}C,2-^{2}H]alanine **1** to an *in vitro* enzyme assay with purified ALT enzyme, demonstrating a kinetic isotope effect, in agreement with prior reports. We anticipate that this versatile method will find application to a variety of substrates for hyperpolarized ^{13}C MRI.

C. T. carried out the experiments and wrote the manuscript with support from D. E. K. R. R. F. and D. M. W. designed and directed the project. H. V. B, D. B. V., S. M. R., R. S. and J. K. helped supervise the project and helped edit the manuscript. C. V. M., J. Y., S. W., J. E. B., S. S. and R. B. helped with characterization of obtained compounds, T_1 measurements and *in vivo* experiments. C. N. and S. M. R. provided critical feedback and helped shape the research, notably for the study of [2-^{13}C,2-^{2}H]enriched substrates.

C. T. acknowledges support from US DOD Prostate Cancer Research Program-Early Investigator Research Award (PC161000). R. R. F. acknowledges support from US DOD Physician Research Training Grant (PC150932), Prostate Cancer Foundation Young Investigator Award and RSNA research fellow award. D. M. W. acknowledges support from NIH grant R01CA166766. D. B. V.,

D. M. W. and S. M. R. acknowledge support from NIH grants P41EB013598, R01CA172845 and R01CA197254.

Conflicts of interest

There are no conflicts to declare.

Notes and references

1 B. M. Goodson, *J. Magn. Reson.*, 2002, **155**, 157–216.
2 N. M. Zacharias, H. R. Chan, N. Sailasuta, B. D. Ross and P. Bhattacharya, *J. Am. Chem. Soc.*, 2012, **134**, 934–943.
3 E. Y. Chekmenev, J. Hövener, V. A. Norton, K. Harris, L. S. Batchelder, P. Bhattacharya, B. D. Ross and D. P. Weitekamp, *J. Am. Chem. Soc.*, 2008, **130**, 4212–4213.
4 S. J. Nelson, J. Kurhanewicz, D. B. Vigneron, P. E. Z. Larson, A. L. Harzstark, M. Ferrone, M. Van Criekinge, J. W. Chang, R. Bok, I. Park, G. Reed, L. Carvajal, E. J. Small, P. Munster, V. K. Weinberg, J. H. Ardenkjaer-larsen, A. P. Chen, R. E. Hurd, L. Odegardstuen, F. J. Robb, J. Tropp and J. A. Murray, *Sci. Transl. Med.*, 2013, **5**, 198ra108.
5 K. Golman, J. H. Ardenkjaer-Larsen, J. S. Petersson, S. Mansson and I. Leunbach, *Proc. Natl. Acad. Sci. U. S. A.*, 2003, **100**, 10435–10439.
6 K. Golman, R. In't Zandt and M. Thaning, *Proc. Natl. Acad. Sci. U. S. A.*, 2006, **103**, 11270–11275.
7 M. J. Albers, R. Bok, A. P. Chen, C. H. Cunningham, M. L. Zierhut, V. Y. Zhang, S. J. Kohler, J. Tropp, R. E. Hurd, Y. F. Yen, S. J. Nelson, D. B. Vigneron and J. Kurhanewicz, *Cancer Res.*, 2008, **68**, 8607–8615.
8 H. Dafni, P. E. Z. Larson, S. Hu, H. A. I. Yoshihara, C. S. Ward, H. S. Venkatesh, C. Wang, X. Zhang, D. B. Vigneron and S. M. Ronen, *Cancer Res.*, 2010, **70**, 7400–7410.
9 S. E. Day, M. I. Kettunen, F. A. Gallagher, D.-E. Hu, M. Lerche, J. Wolber, K. Golman, J. H. Ardenkjaer-Larsen and K. M. Brindle, *Nat. Med.*, 2007, **13**, 1382–1387.
10 J. H. Ardenkjaer-Larsen, B. Fridlund, A. Gram, G. Hansson, L. Hansson, M. H. Lerche, R. Servin, M. Thaning and K. Golman, *Proc. Natl. Acad. Sci. U. S. A.*, 2003, **100**, 10158–10163.
11 P. Bhattacharya, E. Y. Chekmenev, W. F. Reynolds, S. Wagner, N. Zacharias, H. R. Chan, R. Bünger and B. D. Ross, *NMR Biomed.*, 2011, **24**, 1023–1028.
12 A. M. Coffey, R. V. Shchepin, M. L. Truong, K. Wilkens, W. Pham and E. Y. Chekmenev, *Anal. Chem.*, 2016, **88**, 8279–8288.
13 P. J. Rayner, M. J. Burns, A. M. Olaru, P. Norcott, M. Fekete, G. G. R. Green, L. A. R. Highton, R. E. Mewis and S. B. Duckett, *Proc. Natl. Acad. Sci. U. S. A.*, 2017, **114**, E3188–E3194.
14 K. R. Keshari and D. M. Wilson, *Chem. Soc. Rev.*, 2014, **43**, 1627–1659.
15 C. Hundshammer, S. Düwel, S. S. Köcher, M. Gersch, B. Feuerecker, C. Scheurer, A. Haase, S. J. Glaser, M. Schwaiger and F. Schilling, *ChemPhysChem*, 2017, **18**, 2421.
16 H. Allouche-Arnon, A. Gamliel, C. M. Barzilay, R. Nalbandian, J. M. Gomori, M. Karlsson, M. H. Lerche and R. Katz-Brull, *Contrast Media Mol. Imaging*, 2011, **6**, 139–147.
17 S. Meier, M. Karlsson, P. R. Jensen, M. H. Lerche and J. Ø. Duus, *Mol. BioSyst.*, 2011, **7**, 2834.
18 D. E. Korenchan, C. Taglang, C. von Morze, J. E. Blecha, J. W. Gordon, R. Sriram, P. E. Z. Larson, D. B. Vigneron, H. F. VanBrocklin, J. Kurhanewicz, D. M. Wilson and R. R. Flavell, *Analyst*, 2017, **142**, 1429–1433.
19 D. M. Wilson, R. E. Hurd, K. Keshari, M. Van Criekinge, A. P. Chen, S. J. Nelson, D. B. Vigneron and J. Kurhanewicz, *Proc. Natl. Acad. Sci. U. S. A.*, 2009, **106**, 5503–5507.
20 A. K. Grant, E. Vinogradov, X. Wang, R. E. Lenkinski and D. C. Alsop, *Magn. Reson. Med.*, 2011, **66**, 746–755.
21 H. Allouche-Arnon, T. Wade, L. F. Waldner, V. N. Miller, J. M. Gomori, R. Katz-Brull and C. A. McKenzie, *Contrast Media Mol. Imaging*, 2013, **8**, 72–82.
22 A. W. Barb, S. K. Hekmatyar, J. N. Glushka and J. H. Prestegard, *J. Magn. Reson.*, 2013, **228**, 59–65.
23 T. Doura, R. Hata, H. Nonaka, K. Ichikawa and S. Sando, *Angew. Chem., Int. Ed.*, 2012, **51**, 10114–10117.
24 C. Laustsen, G. Pileio, M. C. D. Tayler, L. J. Brown, R. C. D. Brown, M. H. Levitt and J. H. Ardenkjaer-Larsen, *Magn. Reson. Med.*, 2012, **68**, 1262–1265.
25 B. W. C. Kennedy, M. I. Kettunen, D. E. Hu and K. M. Brindle, *J. Am. Chem. Soc.*, 2012, **134**, 4969–4977.
26 K. N. Timm, J. Hartl, M. A. Keller, D. E. Hu, M. I. Kettunen, T. B. Rodrigues, M. Ralser and K. M. Brindle, *Magn. Reson. Med.*, 2015, **74**, 1543–1547.
27 M. Mishkovsky, B. Anderson, M. Karlsson, M. H. Lerche, A. D. Sherry, R. Gruetter, Z. Kovacs and A. Comment, *Sci. Rep.*, 2017, **7**, 11719.
28 H. Nonaka, R. Hata, T. Doura, T. Nishihara, K. Kumagai, M. Akakabe, M. Tsuda, K. Ichikawa and S. Sando, *Nat. Commun.*, 2013, **4**, 1–7.
29 H. Nonaka, M. Hirano, Y. Imakura, Y. Takakusagi, K. Ichikawa and S. Sando, *Sci. Rep.*, 2017, **7**, 1–6.
30 R. V. Shchepin, A. M. Coffey, K. W. Waddell and E. Y. Chekmenev, *Anal. Chem.*, 2014, **86**, 5601–5605.
31 J. Atzrodt, V. Derdau, T. Fey and J. Zimmermann, *Angew. Chem., Int. Ed.*, 2007, **46**, 7744–7765.
32 C. Taglang, L. M. Martínez-Prieto, I. Del Rosal, L. Maron, R. Poteau, K. Philippot, B. Chaudret, S. Perato, A. Sam Lone, C. Puente, C. Dugave, B. Rousseau and G. Pieters, *Angew. Chem., Int. Ed.*, 2015, **54**, 10474–10477.
33 T. Maegawa, Y. Fujiwara, Y. Inagaki, Y. Monguchi and H. Sajiki, *Adv. Synth. Catal.*, 2008, **350**, 2215–2218.
34 Y. Sawama, Y. Monguchi and H. Sajiki, *Synlett*, 2012, 959–972.
35 A. Michelotti, F. Rodrigues and M. Roche, *Org. Process Res. Dev.*, 2017, **21**, 1741–1744.
36 S. Hu, M. Zhu, H. A. I. Yoshihara, D. M. Wilson, K. R. Keshari, P. Shin, G. Reed, C. von Morze, R. Bok, P. E. Z. Larson, J. Kurhanewicz and D. B. Vigneron, *Magn. Reson. Imaging*, 2011, **29**, 1035–1040.
37 J. S. Blicharski, *Z. Naturforsch., A: Phys. Sci.*, 1972, **27**, 1456–1458.
38 F. A. L. Anet and D. J. O'leary, *Concepts Magn. Reson.*, 1992, **4**, 35–52.
39 D. M. Wilson, K. R. Keshari, P. E. Z. Larson, A. P. Chen, S. Hu, M. Van Criekinge, R. Bok, S. J. Nelson, J. M. MacDonald, D. B. Vigneron and J. Kurhanewicz, *J. Magn. Reson.*, 2010, **205**, 141–147.
40 A. W. Barb, S. K. Hekmatyar, J. N. Glushka and J. H. Prestegard, *J. Magn. Reson.*, 2013, **228**, 59–65.
41 J. M. Park, C. Khemtong, S.-C. Liu, R. E. Hurd and D. M. Spielman, *Magn. Reson. Med.*, 2017, **77**, 1741–1748.
42 A. J. L. Cooper, *J. Biol. Chem.*, 1976, **251**, 1088–1096.
43 H. Y. Chen, P. E. Z. Larson, R. A. Bok, C. Von Morze, R. Sriram, R. D. Santos, J. D. Santos, J. W. Gordon, N. Bahrami, M. Ferrone, J. Kurhanewicz and D. B. Vigneron, *Cancer Res.*, 2017, **77**, 3207–3216.

Appendix 2

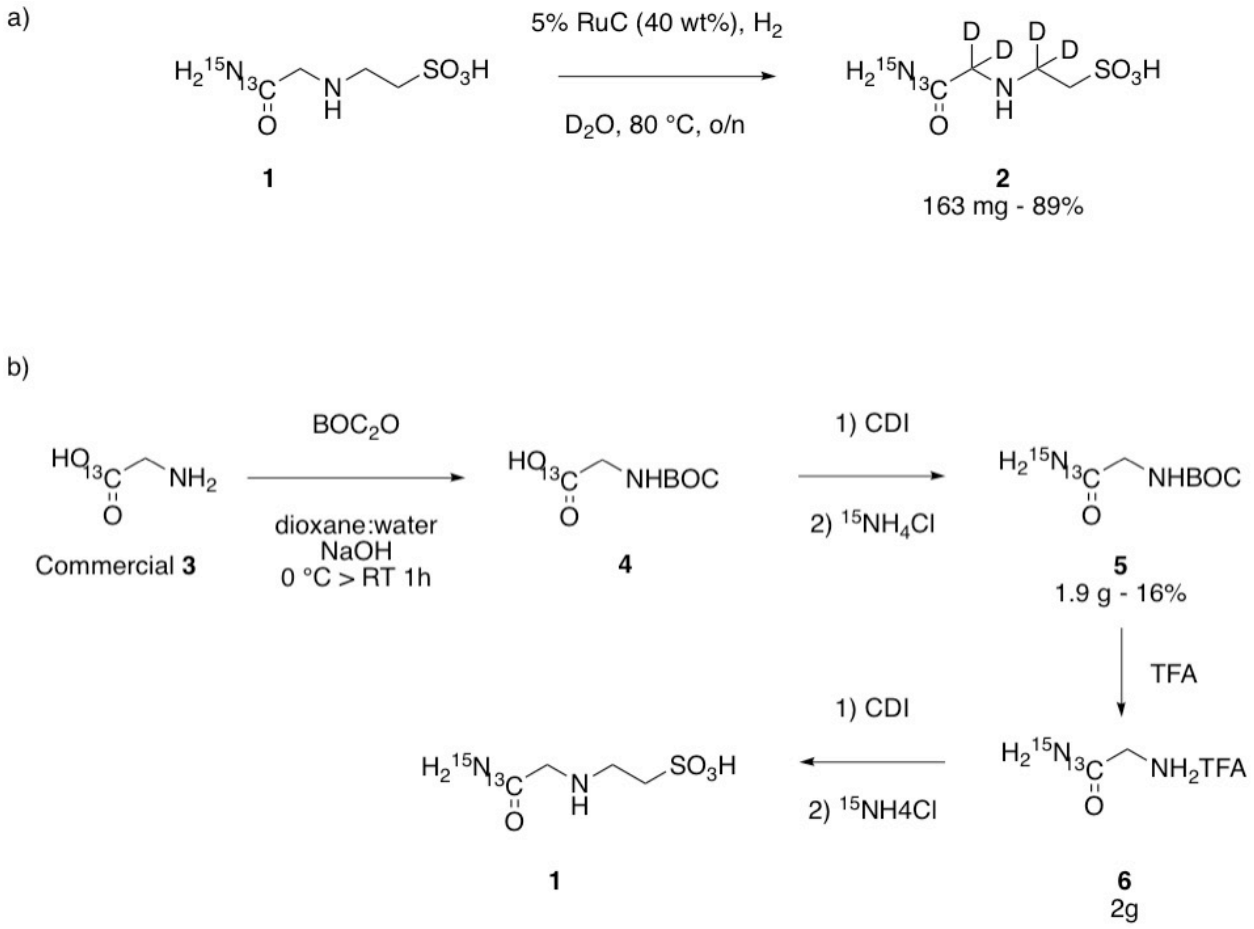

Scheme 1: a) Regioselective catalytic deuterium labelling via $^{1}H/^{2}H$ exchange using ruthenium on carbon (RuC) applied on [^{15}N,^{13}C]ACES. b) Synthesis of [^{15}N,^{13}C]ACES.

Appendix 3

Analyst

COMMUNICATION

View Article Online
View Journal | View Issue

Check for updates

Cite this: *Analyst*, 2017, **142**, 1429

Received 13th January 2017,
Accepted 11th March 2017

DOI: 10.1039/c7an00076f

rsc.li/analyst

Dicarboxylic acids as pH sensors for hyperpolarized ^{13}C magnetic resonance spectroscopic imaging†

D. E. Korenchan,[a,b] C. Taglang,[b] C. von Morze,[b] J. E. Blecha,[b] J. W. Gordon,[b] R. Sriram,[b] P. E. Z. Larson,[a,b] D. B. Vigneron,[b] H. F. VanBrocklin,[b] J. Kurhanewicz,[a,b] D. M. Wilson[b] and R. R. Flavell*[b]

Imaging tumoral pH may help to characterize aggressiveness, metastasis, and therapeutic response. We report the development of hyperpolarized [2-^{13}C,D$_{10}$]diethylmalonic acid, which exhibits a large pH-dependent ^{13}C chemical shift over the physiological range. We demonstrate that co-polarization with [1-^{13}C,D$_9$]*tert*-butanol accurately measures pH *via* ^{13}C NMR and magnetic resonance spectroscopic imaging in phantoms.

Introduction

Interstitial acidification, one of the hallmarks of numerous human cancers,[1] has a significant impact on the tumor microenvironment. Upregulation of aerobic glycolysis leads to proton export from tumor cells and extracellular acidification,[2] leading to reduced tumor uptake of chemotherapeutics,[3] decreased antitumor immune cell function,[4] and tumor invasion and metastasis.[5,6] Interestingly, interstitial pH heterogeneity within a tumor may contain important information about tumor behavior, especially considering that tumor cells tend to grow and migrate predominantly along gradients of decreasing pH.[6] These findings suggest that pH imaging approaches may provide valuable information for clinicians wishing to grade and effectively treat tumors.

Many techniques exist for the measurement of interstitial pH *in vivo*,[7] including fluorescence methods,[6,8] positron emission tomography,[9–12] and magnetic resonance (MR) based approaches.[13,14] The two pH imaging modalities best able to capture intratumoral pH heterogeneity with potential for clinical implementation are ^{1}H chemical exchange saturation transfer (CEST) MRI and hyperpolarized (HP) ^{13}C magnetic resonance spectroscopic imaging (MRSI).[7] HP ^{13}C MRSI, enabled by MR signal enhancement on the order of 10^4–10^5 *via* dynamic nuclear polarization (DNP),[15] has enabled the study of several metabolic and transport processes relevant to cancer, and it has been applied to human prostate cancer imaging in phase I clinical trials.[16] To date, the primary HP agent for measuring interstitial pH is ^{13}C-bicarbonate, which represents a ratiometric approach to calculating pH. Because the conjugate acid (H_2CO_3, in rapid equilibrium with CO_2) and base (HCO_3^-) exhibit distinct MR resonances, the ratio of bicarbonate and CO_2 MR signal intensities can be measured in each volume element (voxel) to calculate a pH map using a modified Henderson–Hasselbalch equation.[17] However, the spatial resolution is limited in part by the low signal-to-noise ratio (SNR) of CO_2, which is typically at a concentration an order of magnitude lower than bicarbonate at physiological pH values (pK_a = 6.17 at 37 °C).[17,18] Recently, a new class of chemical shift (CS) pH probes has been reported, in which the protonated and deprotonated forms of the molecule give rise to a single MR resonance rather than two. Such HP molecules, which include ^{15}N-pyridine derivatives,[19] imidazole-$^{15}N_2$,[20] and ^{13}C-*N*-(2-acetamido)-2-aminoethanesulfonic acid (ACES),[21] may circumvent the low SNR concerns regarding the quantification of two peak intensities.

Some dicarboxylic acids are known to have second pK_a values in the physiological range,[22] as well as carbon nuclei with long T_1 relaxation time constants, making them suitable for pH imaging *via* HP ^{13}C MRSI. Therefore, the goal of this work was to identify a dicarboxylic acid that could be hyperpolarized and used for accurate pH measurement with ^{13}C MRSI.

Experimental

Full experimental details can be found in the ESI.†

Dicarboxylate screening

Eleven dicarboxylates without isotopic labeling were initially screened to measure their pH-dependent ^{13}C chemical shifts

[a]*UC Berkeley-UCSF Graduate Program in Bioengineering, University of California, Berkeley and University of California, San Francisco, California, USA*
[b]*Department of Radiology and Biomedical Imaging, University of California, San Francisco, California, USA. E-mail: Robert.flavell@ucsf.edu*

†Electronic supplementary information (ESI) available: Full experimental details, details on chemical synthesis, and molecular characterization. See DOI: 10.1039/c7an00076f

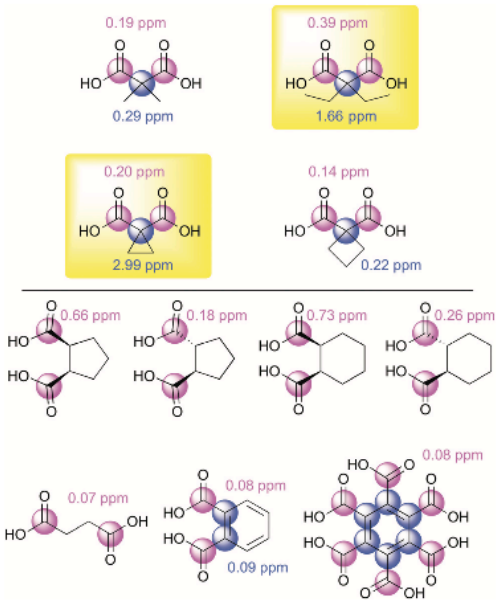

Fig. 1 Investigation of dicarboxylates as ^{13}C MR pH sensors. The downfield CS migration from pH 6.5 to 7.4 is listed near each labelled ^{13}C nucleus. Two molecules with large CS migration over this pH range are highlighted in yellow: diethylmalonic acid (top right) and cyclopropane-1,1-dicarboxylic acid (lower left). Literature pK_a values for these molecules can be found in the ESI.†

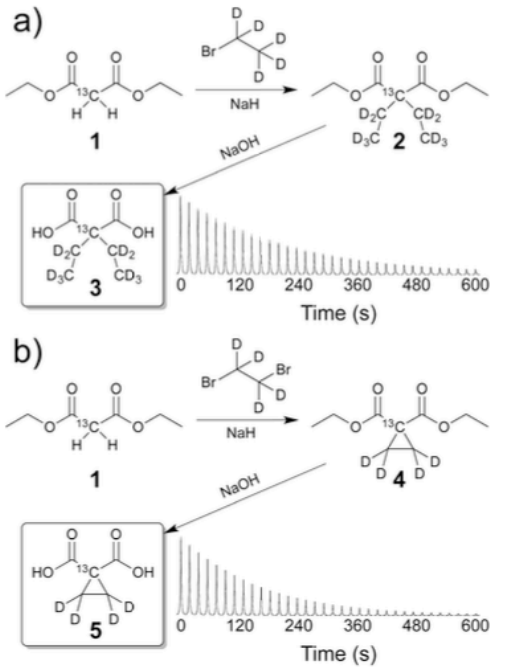

Fig. 2 Synthesis schemes and representative HP ^{13}C T_1 decay curves at 11.7 T for (a) [2-^{13}C,D$_{10}$]diethylmalonic acid (DEMA) **3**, and (b) [2-^{13}C,D$_4$]cyclopropane-1,1-dicarboxylic acid (CPDA) **5**. The measured T_1 values at 11.7 T for DEMA and CPDA were 105.6 ± 5.2 s and 70.2 ± 4.5 s, respectively (n = 3 each).

(Fig. 1). Aqueous solutions of these compounds were prepared, containing 250 mM dicarboxylate and 250 mM urea (CS standard), and the pH was carefully adjusted with HCl or NaOH to either 6.5 or 7.4 using a standard laboratory pH meter. The ^{13}C NMR spectra were acquired at 11.7 T and 37 °C and referenced to urea at 163.7 ppm, and the CS change between these two pH values was measured.

Synthesis of [2-^{13}C,D$_{10}$]diethylmalonic acid and [2-^{13}C,D$_4$] cyclopropane-1,1-dicarboxylic acid

Based on the pH-dependent ^{13}C chemical shifts obtained, enriched syntheses of both [2-^{13}C,D$_{10}$]diethylmalonic acid (DEMA) and [2-^{13}C,D$_4$]cyclopropane-1,1-dicarboxylic acid (CPDA) were performed (Fig. 2). Brief synthetic routes are described below, based on previously described methods.[23] *[2-^{13}C,D$_{10}$]diethylmalonic acid*: [2-^{13}C]diethylmalonate was alkylated with [D$_5$]bromoethane and saponified using NaOH. *[2-^{13}C,D$_4$]cyclopropane-1,1-dicarboxylic acid*: similar to the above, but [D$_4$]1,2-dibromoethane was used in place of [D$_5$] bromoethane. All compounds were characterized *via* standard methods, as described in the ESI.†

Hyperpolarization and characterization of ^{13}C dicarboxylate pH sensors

Enriched ^{13}C dicarboxylate sensors were hyperpolarized *via* the dynamic nuclear polarization (DNP) technique and their solution-state T_1 time constants were determined. ~3.8 M DEMA in *N*,*N*-dimethylacetamide was prepared with 15 mM of OX063 trityl radical and 2 mM Gd-DOTA and co-polarized with *tert*-butanol (*t*BuOH), which was formulated with OX063 in glycerol as previously described.[24] ~4 M CPDA in dimethyl sulfoxide was prepared with 15 mM OX063 trityl radical. After dissolution and NaOH titration (pH 6.6–7.5, both compounds), the HP solution-state T_1 values were determined *via* dynamic ^{13}C MRS (5° hard pulses, flip angle correction, TR = 3 s, n = 3) at 11.7 T and 37 °C.

Titration curve for ^{13}C-enriched DEMA

Based on the T_1 data obtained for ^{13}C DEMA, we obtained an NMR titration curve for this compound in preparation for imaging studies. 5 mM solutions of [2-^{13}C,D$_{10}$]DEMA and [1-^{13}C,D$_9$]*t*BuOH were prepared ranging from pH 2.5 to 8.8. The CS difference between the labeled carbons was measured at 11.7 T and 37 °C, plotted *versus* pH, and fitted to a sigmoi-

dal curve[13] to obtain an MR titration curve. This MR titration curve was used to calculate the pH for HP spectroscopy and phantom experiments using the ^{13}C Δ ppm.

pH imaging phantom

Phantom studies were performed to investigate the use of HP DEMA for pH imaging. HP DEMA and *t*BuOH were diluted to ~5 mM each and titrated in five separate tubes to various pH values at about 37 °C. The phantom was imaged with a ^{13}C 2D CSI sequence (10 × 10 matrix, 10° hard pulses, 7.5 mm isotropic in-plane resolution) on a clinical 3 T MRI scanner. After imaging, dynamic ^{13}C NMR spectroscopy was performed for 3 T T_1 measurement (10° hard pulses, TR = 3 s, n = 2).

Results & discussion

We investigated several dicarboxylic acids using ^{13}C MRS to identify nuclei that demonstrated a pH-dependent chemical shift (Fig. 1). All the tested compounds had two carboxylic acid groups separated by either one carbon (derivatives of malonic acid) or two carbons. All molecules also had a known or predicted pK_a value close to the physiological range (*i.e.* near 7–7.4) and contained at least one carbon nucleus without directly bonded protons, making them likely to have long T_1 relaxation time constants amenable to use with hyperpolarized imaging.[25] Strikingly, the intermediate carbons of all malonic acid derivatives in this study demonstrated larger pH-dependent chemical shifts than did the carboxylic acid carbons themselves. This finding was somewhat surprising, considering that the carbonyl carbons are closer in proximity to the acidic protons in each molecule. Two of the malonic acid derivatives, highlighted in yellow in Fig. 1, demonstrated large chemical shifts over the tested pH range: diethylmalonic acid (DEMA) and cyclopropane-1,1-dicarboxylic acid (CPDA). Of the compounds with two carbons separating the dicarboxylic acid moieties, the *cis* enantiomers demonstrated larger pH-dependent chemical shifts than the *trans*. However, these molecules exhibited smaller pH-dependent carbonyl chemical shifts than the quaternary carbons in the malonates.

Following the dicarboxylate investigation, two-step synthetic routes were developed for the isotopically-enriched, deuterated versions of DEMA and CPDA (Fig. 2). These syntheses were based on a previously reported method applied to valproic acid.[23] In addition to ^{13}C labeling the pH-sensitive quaternary carbon, the functional groups were deuterated for each molecule in order to lengthen the ^{13}C T_1.[25] The overall reaction yields were 64% for DEMA and 45% for CPDA. The reaction products were confirmed to be the target molecules by both NMR (^1H, ^{13}C) and high-resolution mass spectroscopy (see the ESI†). Based upon a preliminary T_1 comparison between the two synthesized compounds (Fig. 2), we chose DEMA for further development as a hyperpolarized pH probe.

The pH-dependent chemical shift behavior of the DEMA quaternary carbon was characterized *via* NMR spectroscopy (Fig. 3a). The CS difference between DEMA and *tert*-butanol (*t*BuOH) was plotted against the pH and fitted to a sigmoidal

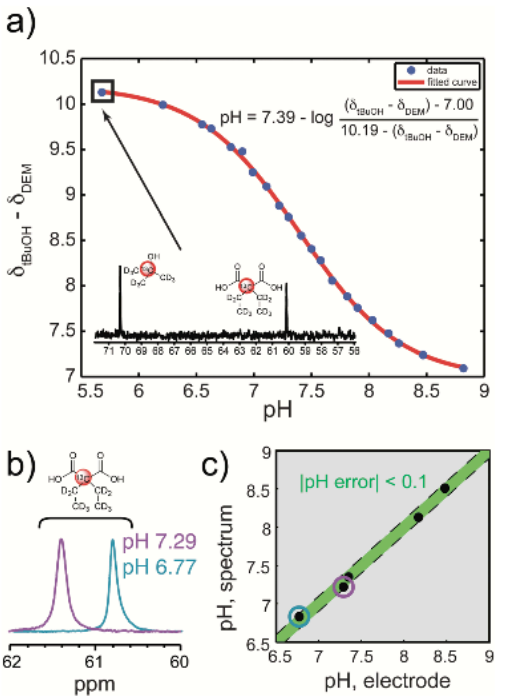

Fig. 3 (a) MR pH titration curve for [2-^{13}C,D_{10}]DEMA. CS difference between DEMA and *t*BuOH is plotted against pH, and the best-fit equation to the data is displayed. Inset: representative ^{13}C MR spectrum of DEMA (upfield) and *t*BuOH (downfield). (b) HP DEMA peak at two pH values (circled points in (c)), demonstrating the pH-dependent chemical shift. Spectra are referenced to *t*BuOH peak. (c) Plot of pH calculated from spectra using equation in (a) *vs.* pH electrode measurements (n = 5). pH values agree within 0.1 pH unit.

curve. The pK_a value was determined to be 7.39 under these conditions, similar to the reported value of 7.29.[26] This slight difference may be attributable to temperature and/or isotopic enrichment. We demonstrated that the NMR titration curve could be used to measure the solution pH from the HP spectra of the co-polarized DEMA and *t*BuOH (Fig. 3b). The pH measured from the HP spectra was within 0.1 pH unit of the pH measured with a conventional pH electrode (Fig. 3c, n = 5). The solution-state polarization, back-calculated to the time of dissolution, was 13.7 ± 0.6% (n = 3). The T_1 values for the HP signal at 3 T and 11.7 T were 84.3 ± 1.4 s (n = 2) and 105.6 ± 5.2 s (n = 3), respectively. The T_1 was longer at the higher field strength, as might be expected for a quaternary carbon nucleus dominated by dipole–dipole relaxation.[27] Minimal variation in T_1 was observed over the physiological pH range (Fig. S1†). The HP DEMA linewidth broadened due to chemical exchange as pH increased from 6.8 (13.1 Hz) to 7.5 (18.7 Hz), as expected based on the exchange mechanism, which is both acid- and base-catalyzed.[28,29]

In order to demonstrate that HP DEMA could be used with spectroscopic imaging techniques, we performed an imaging phantom experiment on a clinical 3 T MRI scanner. This allowed us to measure the pH simultaneously in several solutions (Fig. 4a). As before, the pH in three of five tubes was measured by using the CS difference between the HP DEMA and *t*BuOH peaks (Fig. 4b), and these pH values agreed with electrode measurements within 0.1 pH units (Fig. 4c). Two tubes had pH values at the high and low ends of the measurable pH range. However, the extremely high and extremely low pH tubes demonstrated CS differences of 6.9 and 10.3 ppm, respectively, which agree with the minimum and maximum ppm values determined for the titration curve shown in Fig. 3a.

The HP agents developed in this work, in addition to others reported previously,[19–21] represent a departure from previous techniques in HP pH imaging using ^{13}C-bicarbonate. Important similarities exist between ^{13}C pH agents that are "ratiometric" (*e.g.* ^{13}C-bicarbonate[17]), which quantify pH using the intensities of two separate ^{13}C NMR resonances, and "chemical-shift" (*e.g.* ACES,[21] DEMA), which quantify pH based upon a change in the observed ^{13}C NMR frequency. In both cases, the pH-sensing molecule exists in both a protonated state and a deprotonated state, and the molecule exchanges between the two states with an overall first-order rate constant, k, representing both the forward and reverse reaction rates. The ratiometric and chemical-shift sensors differ in the magnitude of the exchange rate constant, k, relative to the CS dispersion, Δf.[30] For ratiometric pH sensors, the exchange is much slower relative to the CS dispersion ($k \ll \Delta f$), leading to the observation of two distinct resonances *via* MR spectroscopy. In the case of ^{13}C-bicarbonate, the resonances for bicarbonate and CO_2 are separated by a large CS difference of 35.5 ppm. Furthermore, the chemical exchange between the two states is rate-limited by CO_2 hydration to form bicarbonate.[31] Conversely, simple protonation–deprotonation of ACES or DEMA is fast relative to the total CS dispersion over all pH values ($k \gg \Delta f$), as is generally the case for these reactions.[28] Therefore, these molecules exhibit one MR resonance, with a chemical shift that is a weighted average of the chemical shifts of the protonated and deprotonated molecular states.

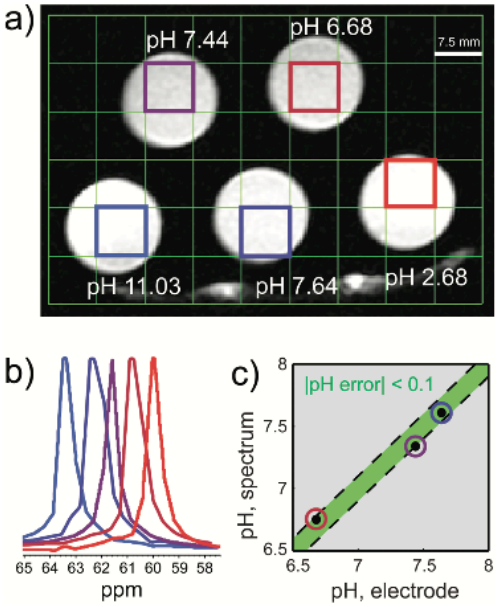

Fig. 4 HP phantom imaging with [2-^{13}C,D$_{10}$]DEMA: (a) T_2-weighted ^{1}H image of tubes containing ~5 mM co-polarized DEMA and *t*BuOH at varying pH values. Electrode pH measurements are displayed near each tube. (b) Overlaid ^{13}C spectra from color-coded voxels, highlighting pH-dependent DEMA chemical shift observed *via* imaging. Spectra are referenced to *t*BuOH peak. (c) Plot of pH values calculated from spectra in (b) *vs.* electrode measurements, demonstrating agreement within 0.1 pH unit. The highest and lowest pH values are not plotted but demonstrated chemical shifts very close to the minimum and maximum CS differences, respectively, seen in the MR titration curve in Fig. 3a.

MR chemical-shift sensors of pH possess certain advantages and disadvantages relative to ratiometric sensors. The presence of a single peak is a significant benefit concerning high spatial resolution imaging, since all HP molecules contribute to the magnitude of the single peak, and because imaging resolution is not limited by the signal of the lower of two peaks. However, these sensors also possess significant challenges. The resonant frequency, which gives a readout of pH, is also sensitive to main magnetic field inhomogeneity and changes in susceptibility throughout the imaging volume. These effects can be accounted for by co-injecting a pH-insensitive HP molecule, in our case *t*BuOH, that is used as a chemical shift reference. Our experimental results in phantoms demonstrate that we can use this approach for highly accurate pH imaging. The ability to resolve different pH values *in vivo* will depend upon image acquisition parameters, voxel size, and B_0 inhomogeneity within each voxel. High-resolution pH imaging, which may be achievable using DEMA, should provide relevant data about pH gradients within tissue. As is the case with other magnetic resonance-based pH imaging approaches,[21,32] the buffering capacity of DEMA could potentially alter the tissue pH. However, the signal gains resulting from hyperpolarization, and from the chemical shift imaging based approaches compared with those from a ratiometric approach, have the potential to minimize these effects.

DEMA exhibits some striking properties that make it amenable to high spatial resolution imaging. Firstly, the T_1 relaxation time constant is one of the longest measured for HP ^{13}C compounds.[25] Interestingly, the T_1 increases with field strength, as opposed to the vast majority of HP compounds ^{13}C-enriched at carbonyls, whose relaxation is dominated by chemical shift anisotropy. However, the T_1 is still exceptionally long at a clinical field strength of 3 T. Combined with the high polarization obtainable for this compound, the long T_1 offers significant flexibility in terms of spatial resolution and timing of HP imaging.

Conclusions

We report a novel compound for pH measurement *via* ^{13}C MRSI, [2-^{13}C,D_{10}]diethylmalonic acid (DEMA). The pH is measured *via* changes in the NMR chemical shift, potentially circumventing SNR limitations found with the HP bicarbonate. The HP imaging pH accuracy and long T_1 values make DEMA a strong potential candidate for high spatial resolution *in vivo* pH mapping.

Acknowledgements

This research was supported by the National Institutes of Health (R01-CA166766), the Education and Research Foundation for Nuclear Medicine and Molecular Imaging (SNMMI-ERF Mitzi and William Blahd, MD, Pilot Grant), the Radiological Society of North America (RSNA Research Fellow Grant), and the Department of Defense (Physician Research Training Grant PC150932). D. E. K. wishes to acknowledge Sukumar Subramaniam for his advice and guidance on imaging strategies and troubleshooting.

Notes and references

1 J. L. Wike-Hooley, J. Haveman and H. S. Reinhold, *Radiother. Oncol.*, 1984, **2**, 343–366.
2 R. A. Gatenby and R. J. Gillies, *Nat. Rev. Cancer*, 2004, **4**, 891–899.
3 B. A. Webb, M. Chimenti, M. P. Jacobson and D. L. Barber, *Nat. Rev. Cancer*, 2011, **11**, 671–677.
4 S. Y. C. Choi, C. C. Collins, P. W. Gout and Y. Wang, *J. Pathol.*, 2013, **230**, 350–355.
5 R. A. Gatenby, E. T. Gawlinski, A. F. Gmitro, B. Kaylor and R. J. Gillies, *Cancer Res.*, 2006, **66**, 5216–5223.
6 V. Estrella, T. Chen, M. Lloyd, J. Wojtkowiak, H. H. Cornnell, A. Ibrahim-Hashim, K. Bailey, Y. Balagurunathan, J. M. Rothberg, B. F. Sloane, J. Johnson, R. A. Gatenby and R. J. Gillies, *Cancer Res.*, 2013, **73**, 1524–1535.
7 L. Q. Chen and M. D. Pagel, *Adv. Radiol.*, 2015, **2015**, 1–25.
8 R. Sanders, A. Draaijer, H. C. Gerritsen, P. M. Houpt and Y. K. Levine, *Anal. Biochem.*, 1995, **227**, 302–308.
9 D. A. Rottenberg, J. Z. Ginos, K. J. Kearfott, L. Junck and D. D. Bigner, *Ann. Neurol.*, 1984, **15**, 98–102.
10 A. L. Vāvere, G. B. Biddlecombe, W. M. Spees, J. R. Garbow, D. Wijesinghe, O. A. Andreev, D. M. Engelman, Y. K. Reshetnyak and J. S. Lewis, *Cancer Res.*, 2009, **69**, 4510–4516.
11 R. R. Flavell, C. Truillet, M. K. Regan, T. Ganguly, J. E. Blecha, J. Kurhanewicz, H. F. VanBrocklin, K. R. Keshari, C. J. Chang, M. J. Evans and D. M. Wilson, *Bioconjugate Chem.*, 2016, **27**, 170–178.
12 M. Bauwens, M. De Saint-Hubert, J. Cleynhens, L. Brams, E. Devos, F. M. Mottaghy and A. Verbruggen, *PLoS One*, 2012, **7**, e38428.
13 R. J. Gillies, Z. Liu and Z. Bhujwalla, *Am. J. Physiol.: Cell Physiol.*, 1994, **267**, C195–C203.
14 A. I. Hashim, X. Zhang, J. W. Wojtkowiak, G. V. Martinez and R. J. Gillies, *NMR Biomed.*, 2011, **24**, 582–591.
15 J. H. Ardenkjaer-Larsen, B. Fridlund, A. Gram, G. Hansson, L. Hansson, M. H. Lerche, R. Servin, M. Thaning and K. Golman, *Proc. Natl. Acad. Sci. U. S. A.*, 2003, **100**, 10158–10163.
16 S. J. Nelson, J. Kurhanewicz, D. B. Vigneron, P. E. Z. Larson, A. L. Harzstark, M. Ferrone, M. van Criekinge, J. W. Chang, R. Bok, I. Park, G. Reed, L. Carvajal, E. J. Small, P. Munster, V. K. Weinberg, J. H. Ardenkjaer-Larsen, A. P. Chen, R. E. Hurd, L. I. Odegardstuen, F. J. Robb, J. Tropp and J. A. Murray, *Sci. Transl. Med.*, 2013, **5**, 198ra108.
17 F. A. Gallagher, M. I. Kettunen, S. E. Day, D.-E. Hu, J. H. Ardenkjaer-Larsen, R. I. T. Zandt, P. R. Jensen, M. Karlsson, K. Golman, M. H. Lerche and K. M. Brindle, *Nature*, 2008, **453**, 940–943.
18 D. E. Korenchan, R. R. Flavell, C. Baligand, R. Sriram, K. Neumann, S. Sukumar, H. VanBrocklin, D. B. Vigneron, D. M. Wilson and J. Kurhanewicz, *Chem. Commun.*, 2016, **52**, 3030–3033.
19 W. Jiang, L. Lumata, W. Chen, S. Zhang, Z. Kovacs, A. D. Sherry and C. Khemtong, *Sci. Rep.*, 2015, **5**, 9104.
20 R. V. Shchepin, D. A. Barskiy, A. M. Coffey, T. Theis, F. Shi, W. S. Warren, B. M. Goodson and E. Y. Chekmenev, *ACS Sens.*, 2016, **1**(6), 640–644.
21 R. R. Flavell, C. von Morze, J. E. Blecha, D. E. Korenchan, M. Van Criekinge, R. Sriram, J. W. Gordon, H.-Y. Chen, S. Subramaniam, R. A. Bok, Z. J. Wang, D. B. Vigneron, P. E. Larson, J. Kurhanewicz and D. M. Wilson, *Chem. Commun.*, 2015, **51**, 14119–14122.
22 F. C. Nachod, *Determination of organic structures by physical methods*, Academic Press, New York, 1955.
23 C. Servens, C. Filliatre and R. Sion, *J. Labelled Compd. Radiopharm.*, 1985, **22**, 1097–1108.
24 A. K. Grant, E. Vinogradov, X. Wang, R. E. Lenkinski and D. C. Alsop, *Magn. Reson. Med.*, 2011, **66**, 746–755.
25 K. R. Keshari and D. M. Wilson, *Chem. Soc. Rev.*, 2014, **43**, 1627–1659.
26 F. C. Nachod, *Determination of organic structures by physical methods*, Academic Press, New York, 1955.
27 E. D. Becker, R. R. Shoup and T. C. Farrar, *Pure Appl. Chem.*, 1972, **32**, 51–66.
28 M. Eigen, *Angew. Chem., Int. Ed. Engl.*, 1964, **3**, 1–19.
29 R. R. Ernst, G. Bodenhausen and A. Wokaun, *Principles of Nuclear Magnetic Resonance in One and Two Dimensions*, Clarendon Press, 1987.
30 P. J. Hore, *Nuclear Magnetic Resonance*, Oxford University Press Inc, New York, 1995.
31 R. Brinkman, R. Margaria and F. J. W. Roughton, *Philos. Trans. R. Soc. London, Ser. A*, 1934, **232**, 65–97.
32 F. A. Gallagher, M. I. Kettunen and K. M. Brindle, *NMR Biomed.*, 2011, **24**, 1006–1015.

Appendix 4

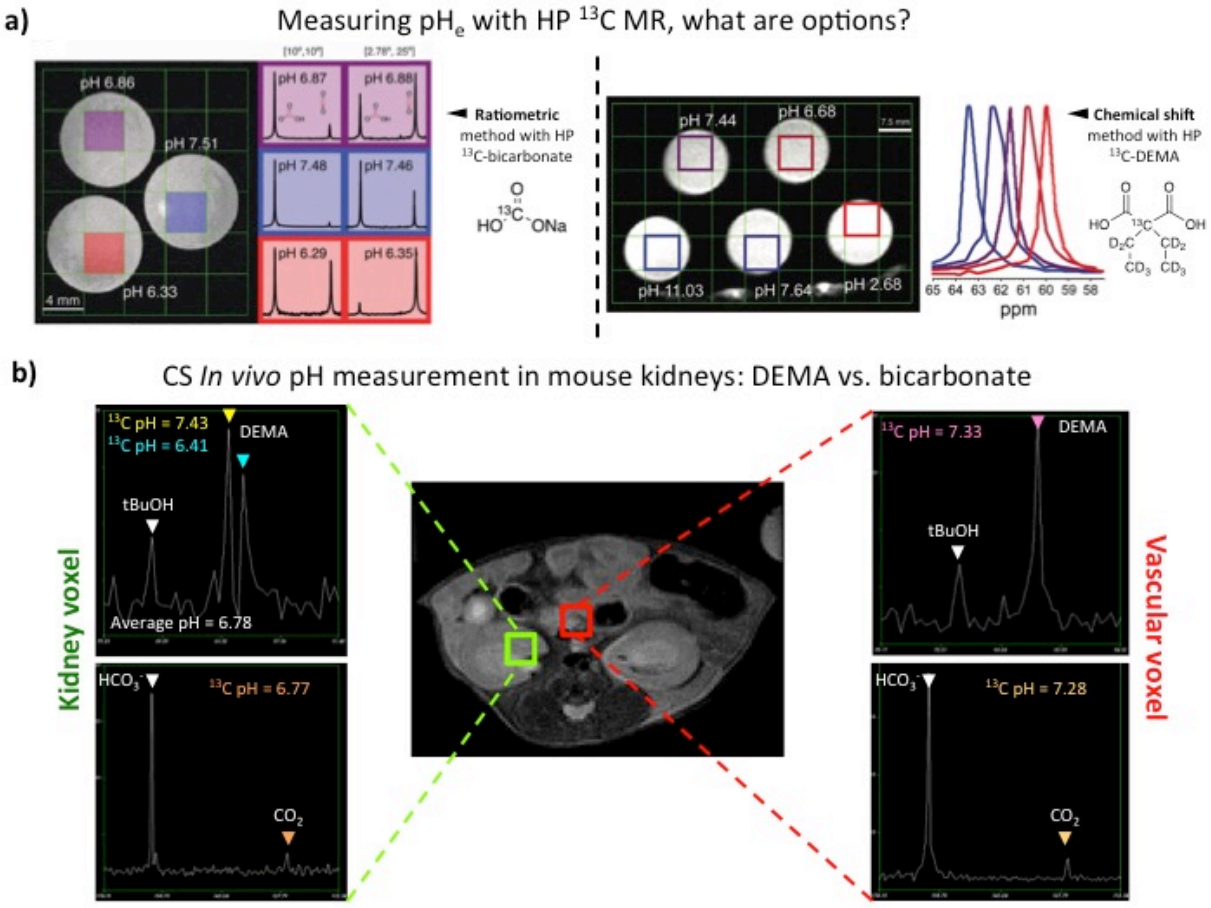

a) Left (*Chem. Commun.* 2016, **52**, 3030): pH phantom results at 14 T of ^{13}C-bicarbonate. T_2-weighted ^{1}H image shows electrode-measured pH values in white. Resonances of $H^{13}CO_3^-$ and $^{13}CO_2$ from HP ^{13}C spectra and calculated pH values for each color-coded voxel were obtained with two excitation pulses. Right (*Analyst*, 2017, **142**, 1429): HP phantom imaging with T_2-weighted ^{1}H image of tubes containing ~5 mM co-polarized DEMA and *t*BuOH at varying pH values. Overlaid ^{13}C spectra from color-coded voxels are referenced to *t*BuOH peak. b) Representative kidney data from a HP ^{13}C measurement in an axial slice overlaid on an anatomical proton image (greyscale). Simultaneously hyperpolarized and injected substances, DEMA and *t*BuOH, show signals in kidneys and blood pool of a healthy mouse. A voxel can contain two pairs of DEMA/*t*BuOH peaks leading to two pH values, contrary to the subsequent injection of ^{13}C-bicarbonate which leads to one pair of $H^{13}CO_3^-/^{13}CO_2$ leading to one mean pH value.

Appendix 5

tBuOH shift (top of the peak)						
165.6	165.6	165.6	165.6	165.6		
165.6	165.6	168.4	168.4			
165.6	165.5	168.4	168.4	168.4		
165.6	165.6	165.6	168.4		165.6	

Delta ppm 1						
				5.2		
		8	7.9			
		7.9	8	7.9		
			8			

Delta ppm 2						
		9.6	9.7	9.7		
			9.6			

pH 1						
			7.37			
		7.29	7.29	7.37		
		7.37	7.29			

pH 2						
		6.28	6.18	6.18		
			6.28			

DEMA shift (top of the peak)						
						160.4
			160.4	160.5	160.5	160.5
		160.1	160.5	160.4	160.5	160.4
				160.4	160.4	

DEMA shift (smaller peak)						
			158.8	158.7	158.7	
				158.8		

delta ppm	delta ppm-7	10.22-delta	r fraction	log fraction	pH
9.7	2.54	0.52	4.884615	0.68883	6.18117

Appendix 6

tBuOH shift (top of the peak)							
168.7	168.7	168.6	168.5	168.4			
168.7	168.7	168.6	168.5	168.4	168.4		
	168.7		168.5	168.5	168.4		

Delta ppm 1							
7.8	8	8.1	8.1	8			
8	8.1	8.2	8.1	8	8		
	8.2		8.1	8.1	8		

Delta ppm 2							
	9.7		9.8	9.7	9.7		
	9.8						

pH 1							
7.45	7.29	7.22	7.22	7.29			
7.29	7.22	7.16	7.22	7.29	7.29		
	7.16		7.22	7.22	7.29		

pH 2							
	6.18		6.07	6.18	6.18		
	6.07						

DEMA shift (top of the peak)							
160.9	160.7	160.5	160.5	160.4	160.4	160.4	160.4
160.7	160.6	160.4	160.4	160.4	160.4	160.4	160.4
160.6	160.5		160.4	160.4	160.4	160.4	160.4

DEMA shift (smaller peak)							
	159		158.7	158.7	158.7		
	158.9						

delta ppm	delta ppm-7.2	10.22-delta ppm	fraction	log fraction	pH
9.8	2.64	0.42	6.285714	0.798355	6.071645